Accepted Manuscript

Plant viral nanoparticles-based HER2 vaccine: Immune response influenced by differential transport, localization and cellular interactions of particulate carriers

Sourabh Shukla, Jay T. Myers, Sarah E. Woods, Xingjian Gong, Anna E. Czapar, Ulrich Commandeur, Alex Y. Huang, Alan Levine, Nicole F. Steinmetz

PII: S0142-9612(16)30749-9

DOI: 10.1016/j.biomaterials.2016.12.030

Reference: JBMT 17879

To appear in: *Biomaterials*

Received Date: 26 October 2016

Revised Date: 18 December 2016

Accepted Date: 27 December 2016

Please cite this article as: Shukla S, Myers JT, Woods SE, Gong X, Czapar AE, Commandeur U, Huang AY, Levine A, Steinmetz NF, Plant viral nanoparticles-based HER2 vaccine: Immune response influenced by differential transport, localization and cellular interactions of particulate carriers, *Biomaterials* (2017), doi: 10.1016/j.biomaterials.2016.12.030.

Plant viral nanoparticles-based HER2 vaccine: Immune response influenced by differential transport, localization and cellular interactions of particulate carriers

Sourabh Shukla[§□]*, Jay T Myers[□], Sarah E Woods[§], Xingjian Gong[§], Anna E. Czapar[§], Ulrich Commandeur[#], Alex Y Huang[□□], Alan Levine[&], Nicole F Steinmetz[§‡□□‖]*

Department of [§]Biomedical Engineering, [‡]Radiology, [□]Materials Science and Engineering, [#]Macromolecular Science and Engineering, [□]Pediatrics, [□]Case Comprehensive Cancer Center, [&]Molecular Biology and Microbiology, [‖]Division of General Medical Sciences-Oncology, Case Western Reserve University, Cleveland, OH 44118. [#]Department of Molecular Biotechnology, RWTH-Aachen University, 52064 Aachen, Germany.

*Co-corresponding authors: sourabh.shukla@case.edu, nicole.steinmetz@case.edu

Abstract:

Cancer vaccines are designed to elicit an endogenous adaptive immune response that can successfully recognize and eliminate residual or recurring tumors. Such approaches can potentially overcome shortcomings of passive immunotherapies by generating long-lived therapeutic effects and immune memory while limiting systemic toxicities. A critical determinant of vaccine efficacy is efficient transport and delivery of tumor-associated antigens to professional antigen presenting cells (APCs). Plant viral nanoparticles (VNPs) with natural tropism for APCs and a high payload carrying capacity may be particularly effective vaccine carriers. The applicability of VNP platform technologies is governed by stringent structure-function relationships. We compare two distinct VNP platforms: icosahedral cowpea mosaic virus (CPMV) and filamentous potato virus X (PVX). Specifically, we evaluate *in vivo* capabilities of engineered VNPs delivering human epidermal growth factor receptor 2 (HER2) epitopes for therapy and prophylaxis of $HER2^{+}$ malignancies. Our results corroborate the structure-function relationship where icosahedral CPMV particles showed significantly enhanced lymph node transport and retention, and greater uptake by/ activation of APCs compared to filamentous PVX particles. These enhanced immune cell interactions and transport properties resulted in elevated HER2-specific antibody titers raised by CPMV- vs. PVX-based peptide vaccine carriers. The 'synthetic virology' field is rapidly expanding with numerous platforms undergoing development and preclinical testing; our studies highlight the need for systematic studies to define rules guiding the design and rational choice of platform, in the context of peptide-vaccine display technologies.

Keywords: Cancer vaccine; viral nanoparticles; HER2; antigen delivery; peptide vaccine

Graphical Abstract

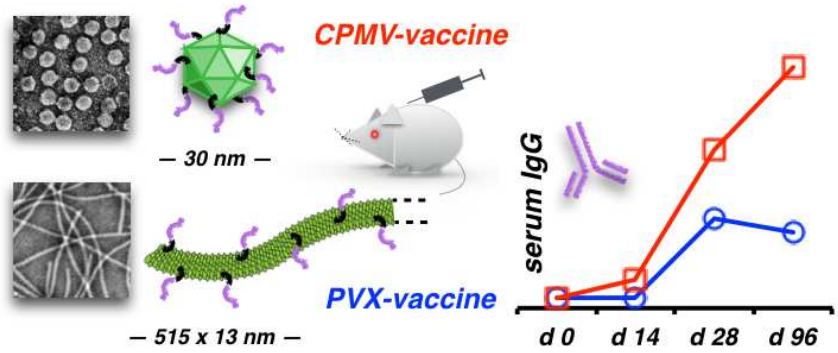

Introduction:

Cancer vaccines are designed to activate or rejuvenate the immune system to recognize tumor-associated antigens and eliminate residual or recurring disease following primary treatments [1-3]. In stimulating a sustained endogenous immune response and resultant memory, cancer vaccines have the potential to overcome the limited, short-term effects associated with passive immunotherapies and the accompanying need for frequent administration at high cost. Passive immunotherapy, often administered systemically, is also associated with development of resistance and toxicities [4, 5].

Several cancer vaccines have already been successfully incorporated in the clinic, and many different approaches are currently under development [3, 6]. Peptide subunit-based vaccines are among the most explored cancer vaccine approaches and rely on the efficient presentation of epitopes to the various components of the immune system, a critical role of vaccine delivery platforms [7-11]. Nanoparticulate carriers are particularly promising candidates capable of delivering high payloads of peptide antigens with enhanced stability and bioavailability [12-14]. Moreover, particulate carriers can provide additional immunostimulatory impetus by engaging pattern recognition receptors on immune cells, thereby enhancing the overall immunogenicity of the vaccine [9, 15].

Plant viral nanoparticles (VNPs) possessing highly ordered and multivalent protein capsids are ideally suited to display repetitive arrays of immunogenic peptide epitopes as vaccine platforms [16-21]. Conceptually different from viral vector platforms that rely on expression of antigenic peptides by antigen presenting cells (APCs) [22-25], VNPs can deliver large payloads of genetically fused or chemically conjugated immunogenic epitopes to a wide range of APCs [18, 26]. In addition, the physical and genetic stability of VNPs and their non-integrating and

non-infectious nature in mammals adds a layer of safety for VNP-based vaccine applications. VNPs can also be engineered to co-deliver other immunostimulatory molecules to improve vaccine efficacy [9, 27].

A unique advantage offered by VNPs as vaccine platforms is their intrinsic immune-stimulatory properties that obviate the need for toxic adjuvants and co-stimulatory molecules [28]. However, the extent and nature of VNP-immune cell interactions has been shown to be dependent on particle morphology and molecular composition. The wide array of different shapes, sizes and aspect ratios (ratio of length and width) of VNPs bring about significant changes in *in vivo* properties and functionality. This strong structure-function relationship determines the suitability of one VNP over another for specific biomedical applications [19, 20, 29, 30]. High aspect ratio nanoparticles offer significantly higher payload carrying capacity, but may also evade phagocytic immune cells (thus providing advantageous properties for drug delivery and imaging applications) [18, 29-31]. Low aspect ratio materials, such as icosahedral platforms, may be beneficial for application as vaccines and immunotherapies [32].

In this study, we set out to evaluate VNP–immune cell interactions, define their fates *in vivo*, and evaluate their potential to trigger a human epidermal growth factor receptor 2 (HER2)-targeted humoral response. We compared two morphologically distinct VNP platforms: the 30 nm icosahedral cowpea mosaic virus (CPMV) and 515 x 13 nm filamentous potato virus X (PVX). Each particle platform was produced through farming in plants and chemically modified to display HER2-specific antigens. The immunological properties of the vaccine formulations were evaluated in tissue culture and in murine models.

We chose CPMV and PVX, because both platforms have been previously studied as vaccine delivery platforms in conjugation with epitopes derived from tumor antigens or

infectious agents, demonstrating efficacy both to prime humoral and cellular responses in the context of cancer [32-38]. For example, PVX coupled with weak idotypic tumor antigen has been shown to induce protective humoral immunity against murine B-cell malignancy [38]. Furthermore, both platforms have been shown to show efficacy when applied as in situ vaccine for treatment of cancer: CPMV stimulates a potent systemic anti-tumor immune response in mouse models of melanoma, ovarian, colon and breast cancer [28]; and we recently demonstrated that PVX also elicits anti-tumor immunity when administered intramurally in a dermal melanoma model [Lee, Murray et al, in review].

We chose to target HER2 positive disease, because HER2 overexpression is associated with aggressive breast cancer (and other malignancies). Patients with this disease have a high incident of metastasis development and relapse [39]. Successful implementation of passive immunotherapy with the HER2-specific monoclonal antibody Herceptin is a testimonial to the potential of antibody-mediated therapeutic intervention [40], and several other B cell epitopes from the extracellular domain of HER2 receptor have been identified and are undergoing testing for vaccine development [41-44]. With the long-term goal to establish a VNP-based HER2 vaccine for treatment of $HER2^+$ patients, either used as a therapeutic or prophylactic vaccine, we initiated this project to assess the suitability of the platform technology, CPMV vs. PVX, for such development.

Results and Discussion:

Propagation and Purification of CPMV and PVX particles: CPMV and PVX particles were propagated and purified using established methods [45]. The isolation of either VNP yielded approximately 1 mg of virus particle per gram of infected leaf material. TEM images show the

distinct morphology of the two particles (Figure 1A). CPMV is a 30 nm-sized nanoparticle (Figure 1A) containing 60 copies each of a large (L, 42 kDa) and small (S, 24 kDa) coat protein arranged with pT=3 icosahedral symmetry. PVX is a flexible filament measuring 515 x 13 nm (Figure 1A) and is composed of 1270 identical copies of a 25-kDa capsid protein. Both CPMV and PVX particles can be stably stored for long periods of time (months-to-years). The physical and genetic stability as well as batch-to-batch structural consistency confer advantageous characteristics for application as a nanocarrier. For cellular uptake studies, fluorescently tagged CPMV and PVX particles were synthesized using established protocols targeting solvent-exposed lysine side chains using NHS-active Alexa Fluor 647 dyes (yielding A647-CPMV and A647-PVX). UV-vis spectroscopy was used to determine the degree of labelling: A647-CPMV was found to display 27 A647 per particle, and A647-PVX was found to display 175 A647 per particle. The 6-fold difference in labelling reflects the 6-fold greater molecular weight of PVX. Thus, the spatial array of fluorophores is displayed at a similar density yielding particles with comparable fluorescent properties.

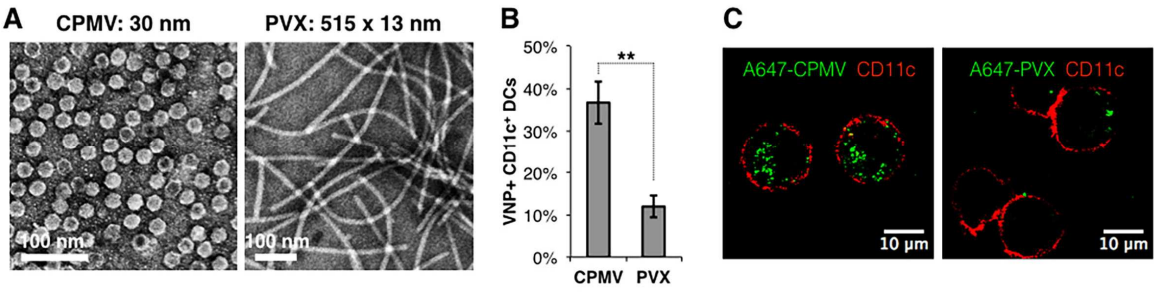

Figure 1. Comparing CPMV and PVX structure and interactions with APCs. (A) TEM images illustrate distinct morphology of CPMV and PVX VNPs. (B) Flow cytometry analysis comparing *in vitro* uptake of A647-CPMV vs. A647-PVX particles following 2 h incubation at 37°C by $CD11c^+$ BMDCs isolated from FVB mice. Student's T test was used for statistical analysis with ** = $p<0.01$. (C) Confocal microscopic images show enhanced uptake of A647-CPMV particles vs. A647-PVX particles (both green) in CD11c stained (red) BMDCs after 2 h incubation.

Determination of VNP–APCs interactions: Interaction with and activation of professional APCs including dendritic cells (DCs) and macrophages are crucial for vaccine efficacy [46-48]. DCs sample antigens, transport immunogenic components (including vaccine carriers) to secondary lymphoid organs, initiate and sustain humoral and/or cellular responses. Thus efficient delivery of antigens to DCs is a critical step in vaccine-mediated immune stimulation. To compare the extent of endocytic uptake by DCs, fluorescently tagged CPMV and PVX particles (A647-CPMV and A647-PVX) were incubated with bone marrow derived DCs (BMDCs) isolated from FVB mice and analyzed using flow cytometry. Percentage of $CD11c^{+}$VNP+ cells was then quantified as a measure of DC uptake (Figure 1B). The results indicated a significantly ($p<0.01$) higher percentage of $CD11c^{+}$ DCs were CPMV+ (36%) vs. PVX+ (12%), suggesting enhanced uptake of CPMV particles by DCs (Figure 1B). The differential uptake was also evident through confocal microscopy, where BMDCs stained with anti-CD11c antibodies showed increased uptake of A647-CPMV particles over A647-PVX particles (Figure 1C).

Uptake of antigens and particulate carriers by APCs depends on several properties including shape, size, surface charge and receptor interactions [49, 50]. The particulate and repetitive nature of VNPs mimics pathogen-associated molecular patterns (PAMPs) which are perceived as danger signals and drive protective immunity [51]. Such molecular patterns are recognized by diverse pattern recognition receptors (PPRs) such as TLR on immune cells, specifically APCs, and facilitate enhanced uptake of nanoparticle-based vaccines by these cells [52, 53]. APCs can internalize particulate carriers by phagocytosis, pinocytosis, or receptor-mediated endocytosis. The observed differences comparing CPMV and PVX may be explained by their different surface chemistry and/ or shape. Phagocytic uptake has been shown to be dependent on particle shape and size, and is likely to render uptake of PVX by DCs inefficient as

compared to CPMV. Low aspect ratio materials, such as CPMV have been shown to exhibit enhanced cell uptake kinetics compared to high aspect ratio materials, such as PVX [54, 55]. Moreover, previous studies have illustrated natural tropism of CPMV toward professional APCs [26]. For example, it has been indicated that CPMV binds to APCs via a 54-kDa cell surface form of the structural protein vimentin, which then facilitates receptor-mediated endocytosis the particle [56-58]. Thus, a combination of efficient endocytosis and receptor-mediated endocytosis together enable enhanced uptake of CPMV by DCs.

We also observed a differential cytokine activation profile for the two particles. BMDCs incubated with equivalent amounts of VNPs (5 μg each of non-fluorescent CPMV and PVX particles) resulted in a significantly higher pro-inflammatory TNF-α and IL-6 response to PVX as compared to CPMV (**Supplementary figure S1**). The proinflammatory cytokine profile is similar to that of bacterial LPS, which engages TLR4 receptors. While this suggests possibility of underlying differences in the interaction and activation of professional APCs by the two vaccine delivery vehicles, given the complexity and diversity of cytokines, a more detailed study encompassing a significantly larger class of molecules is required.

Lymph node trafficking and cellular interaction within the draining lymph node: Following subcutaneous administration of vaccines, trafficking of antigens from peripheral tissues to secondary lymphoid organs, such as draining lymph nodes (dLNs) through the lymphatic system, is critical for development of an adaptive immune response. Nanoparticle carriers could significantly improve transport of subunit vaccines to lymph nodes and facilitate interactions of antigens to the immune system [59]. Size of the carriers is a key design consideration as particles smaller than 100 nm generally enter and drain efficiently in the lymphatic system and can be transported in free form. Larger particles (100-500 nm), on the other hand, are transported less

efficiently and much slower to the lymph nodes – often by phagocytic cells [47, 60]. Here we evaluate whether differences observed in *in vitro* cell uptake studies translate to *in vivo* models.

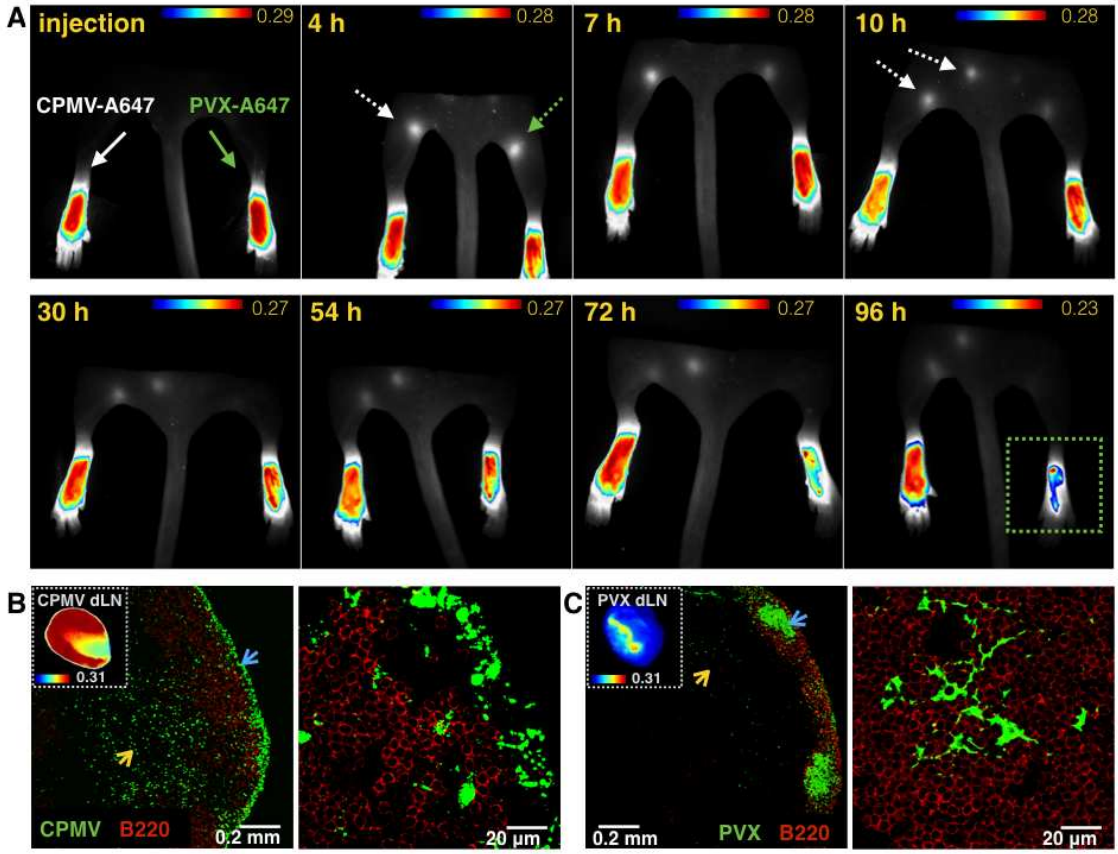

Figure 2. Lymph node trafficking and differential localization of CPMV and PVX particles within the draining lymph node (dLN). (A) Maestro imaging following footpad injection of CPMV-A647 (left footpad) and PVX-A647 (right footpad) in mouse was used to determine trafficking of fluorescent VNPs to corresponding draining lymph nodes (pointed by dotted arrows) over time (A). Maestro imaging (insets) and immunofluorescence staining show differential accumulation and localization of A647-CPMV (B) and A647-PVX (C) particles (green) within draining brachial lymph nodes 12 h following sub-cutaneous administration behind neck in mice. B cells zones (stained with anti-B220 antibody) are showed in red, T cell regions are indicated with yellow arrows. High magnification images showing regions of VNP accumulations (indicated with blue arrows) illustrate localization of A647-CPMV and A647-PVX in subcapsular sinus and B follicle regions, respectively.

In order to observe the kinetics of VNP drainage and retention in dLNs, fluorescent viral carriers were injected subcutaneously into the footpad as it allows for easy tracking of particles

draining to the popliteal lymph nodes [60]. Equal amounts (50 μg each; normalization to amount of protein administered also normalizes the fluorescent payload) of CPMV and PVX carriers were injected as indicated by white and green solid arrows corresponding to CPMV and PVX, respectively, and imaged over time (Figure 2A). Within just 4 h post injection, fluorescence from both CPMV and PVX particles can be observed in the corresponding dLNs indicated by dotted arrows, while a large fraction of injected fluorescent particles are still observed in the footpads. The sustained fluorescent signal from CPMV dLNs and site of injection indicated persistent trafficking and/or retention of CPMV to dLNs for an extended 96 h period as compared to PVX, which begins to be cleared from corresponding dLNs as early as 7-10 h and from the site of injection by 55 h following the injection (Figure 2A). These results clearly indicate differential drainage or retention mechanism of CPMV and PVX particles. We similarly determined dLNs following subcutaneous injections of fluorescent VNPs behind the neck, a site chosen for vaccine administration. Mice immunized s.c. behind the neck with A647-CPMV and A647-PVX particles were euthanized 12 h post injection, then peripheral LNs were harvested and analyzed using the Maestro imaging system (Figure 2B and C). We chose the 12 h time point, because other studies demonstrated that LN accumulation of nanoparticles typically peaks 12 h post dosing [61, 62]. Both CPMV and PVX predominantly localized to the brachial dLNs with fluorescent intensities indicating enhanced accumulation of CPMV particles over PVX, mirroring the results observed via the footpad injections and suggesting differential mechanisms of drainage (insets, Figure 2B and 2C). While freely transporting CPMV particles are likely to reach draining lymph nodes more efficiently over the larger PVX particles, which may drain slower through lymphatic vessels, the sustained presence of CPMV in dLNs suggest enhanced interaction with resident immune cells over PVX. These results are in agreement with the size

dependence of nanoparticle diffusion kinetics through the lymphatic vessels that has been extensively studied [59, 63, 64].

Interestingly, immunofluorescence analysis using confocal microscopy revealed remarkably distinct intra-dLN localization of the two particles: CPMV particles accumulated in large numbers at the subcapsular sinus areas of the dLN, regions populated with subcapsular sinus macrophages (Figure 2B) and T cell zones (yellow arrow). Subcapsular sinus macrophages are the first cells that encounter and phagocytose particulate antigens carried by afferent lymphatics reaching the dLNs, which are subsequently passed on to other APCs for processing and presentation to T cells. The accumulation and trafficking patterns of CPMV within the dLNs are similar to previously reported particulate antigens of comparable sizes [65]. PVX particles, on the contrary, were predominantly sequestered in the B cell follicle zones in the dLNs (Figure 2C). It is apparent that the larger PVX particles are transported less efficiently into the draining lymph nodes. Due to the high aspect ratio, PVX may evade phagocytosis and processing by subcapsular macrophages or other resident APCs, and instead are captured and transported by non-cognate follicular B cells. Follicular B cells have been shown to interact with antigens that diffuse through subcapsular sinus and transport antigens to follicular dendritic cells in the germinal center [65-68]. We have previously observed, similar patterns, as PVX particles accumulates in the B cell follicle regions of the spleen following intravenous injections [20]. While data indicate sequestration in the B cell follicle, uptake into B cells is not observed (Figure 2C). However, proteases in lymphatic fluids have been shown to cleave antigens from nanoparticle carriers and thus facilitate antigen-B cell interactions without the requirement of nanoparticle uptake [69]. Reduced fluorescence in B cell follicle regions at 24 h following dosing may indicate proteolytic processing of PVX (Supplementary figure 2a+b).

Again, the distinct localization and transport of CPMV and PVX within dLN can be attributed to their molecular or morphological differences or a combination of both. These differences are likely to result in distinct pathways of immune stimulation and therefore may influence the nature and extent of immune response triggered by the two distinct vaccination platforms.

We further investigated the interactions of VNPs with various APCs within the dLN. Total vs. VNP^+ immune cell populations ($CD11c^+$ DCs, $F/480^+$ macrophages and $CD19^+$ B cells) from dLNs were analyzed by flow cytometry and compared to brachial LNs from naïve mice (Figure 3). Total $CD11c^+$ DC population did not change significantly between naïve and immunized dLNs over time, indicating no significant influx of DCs into the LNs following the administration and trafficking of VNPs. However, the resident DC population does show varying degrees of CPMV and PVX uptake with time (Figure 3A). In CPMV-administered mice the VNP^+ fractions were 36%, 56%, and 43% at 12 h, 24 h and 48 h post-injection, indicating a continuous and sustained influx of CPMV particles through lymphatic drainage, which peaks at 24 h. In PVX-administered mice the VNP^+ fractions remained low (11%, 23% and 3% at 12 h, 24 h, and 48 h post-injection), indicating lower association of PVX particles with $CD11c^+$ DCs (Figure 3A). These results mirror the *in vitro* results showing significantly lower uptake of PVX particles by BMDCs and the lymph node trafficking results that indicated rapid clearance of PVX from the dLN versus the prolonged presence of CPMV seen in the dLNs injected mice (Figure 2A).

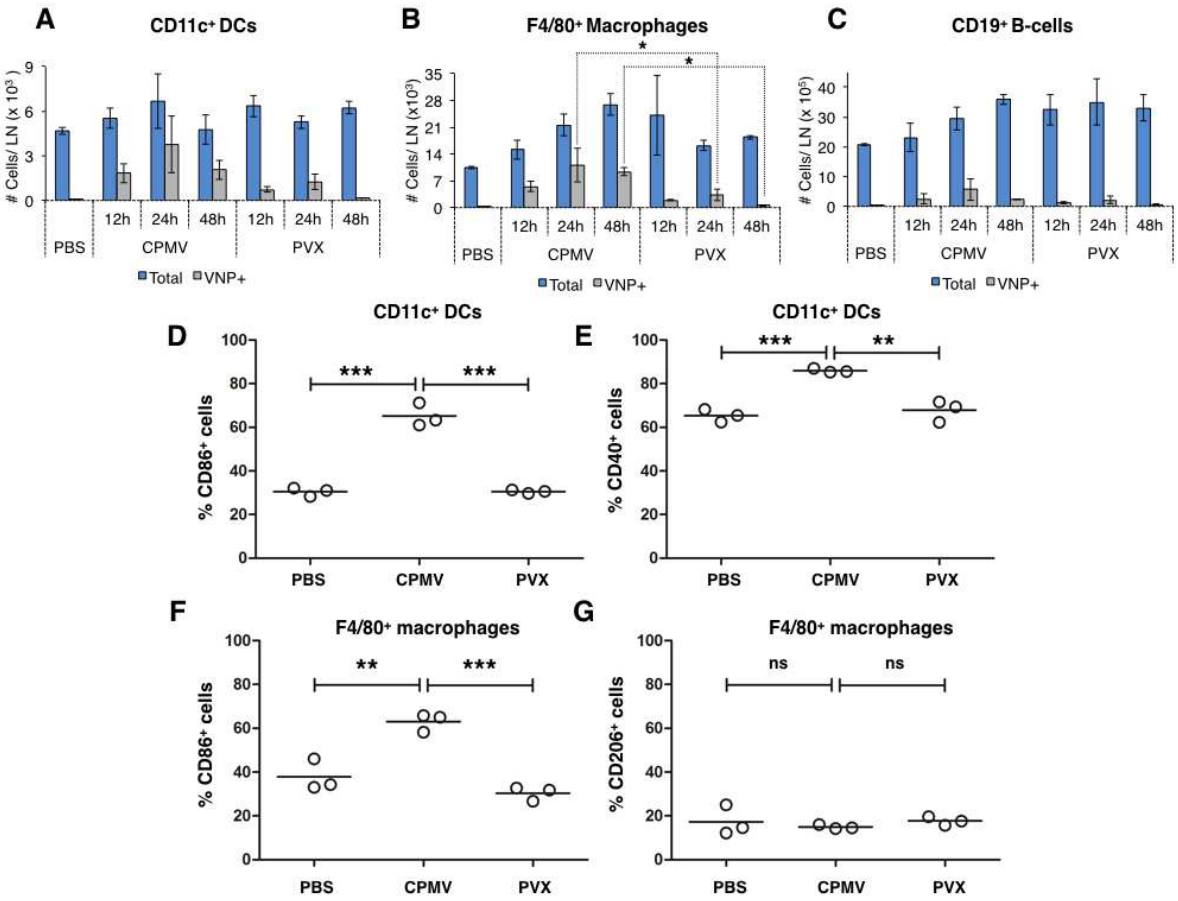

Figure 3. Cellular interactions of VNP carriers within the draining lymph nodes. (A-C) Flow cytometry analysis of digested LN cells was used to determine interactions of CPMV and PVX particles with CD11c$^+$ DCs, F4/80$^+$ macrophages and CD19$^+$ B cells at 12 h, 24 h and 48 h following particle administration. Statistical analysis was performed using one-way ANOVA followed by Bonferroni correction using GraphPad Prism software. (D-G) Flow cytometry analysis was also used to determine activation of CD11c$^+$ DCs and F4/80$^+$ macrophages from digested dLNs 24 h following VNP administration.

The F4/80$^+$ macrophage population showed increased accumulation in the dLN post treatment with either CPMV or PVX compared to naïve mice (this was observed at 24 h and 48 h post injection), indicating increased influx of phagocytic macrophages (Figure 3B). Again, CPMV showed significantly higher interaction with the F4/80$^+$ cells over PVX at 24 h and 48 h post injection (51% vs. 20% at 24 h and 35% vs. 3% at 48 h for CPMV and PVX, respectively) (Figure 3B). A similar increase was observed for CD19$^+$ B cells that showed elevated influx into

dLNs after VNP immunization (Figure 3C). However, both CPMV and PVX showed lower interactions with B cells as compared to DCs and macrophage cell populations, consistent with their role as the primary APCs in the dLNs. Further analysis of the activation status of $CD11c^+$ DCs and $F4/80^+$ macrophages within the dLNs resulting from these interactions with carrier VNPs was performed. Our results indicated significantly higher expression of CD86 and CD40 co-stimulatory markers on $CD11c^+$ DCs in the dLN of mice injected with CPMV as compared to PVX injected mice (Figure 3D, E). Increased expression of CD86, CD40, and several other cell surface markers is associated with APCs maturation and is a critical step leading to a cascade of immunostimulatory effects [70, 71]. Similarly, CPMV positive $F4/80^+$ macrophages showed significantly elevated expression of CD86 co-stimulatory molecule over PVX positive macrophage population (Figure 3F). Elevated CD86 expression in macrophage population together with absence of any significant CD206 expression over control population (Figure 3G) implies activation of a classical M1 phenotype and absence of the alternatively activated regulatory M2 phenotype [72].

Together, our results suggest that following subcutaneous administration, CPMV particles are more efficiently drained into LN compared to PVX. We hypothesize that the high aspect ratio of PVX not only impedes lymphatic drainage, but also influences the degree of interactions with resident immune cell populations, as indicated by immunofluorescence and flow cytometry data. Thus, while CPMV particles undergo macrophage- and DC-mediated uptake and processing, PVX is sequestered in B cell rich follicles regions (however, it should be noted that uptake into B cells was not apparent), overall indicating a more favorable immune activation profile of CPMV over PVX carrier for vaccine applications.

Design of CPMV- and PVX-based HER2 vaccine: To test whether enhanced lymphatic drainage and uptake by APCs of CPMV vs. PVX, translate to enhanced humoral immune stimulation against cancer-specific epitopes, we designed and tested HER2 vaccine formulations. CPMV and PVX based HER2 vaccine formulations were designed to display multiple copies of validated immunodominant epitopes derived from distinct regions of the HER2 extracellular domain:

$CH401_{163-182}$ (YQDTILWKDIFHKNNQLALT) and

$P4_{378-398}$ (PESFDGDPASNTAPLQPEQLQ).

Both CH401 and P4 have been validated in preclinical studies, and peptide formulations are subjects of several ongoing clinical trials assessing their safety and efficacy in the setting of $HER2^+$ disease [73-75]. Here, the peptides CH401 and P4 were designed with a C-terminal cysteine residue to enable chemical coupling to the VNP carrier via an intervening GPSL linker [76] (Figure 4A). We also tested the design of vaccine candidates using an intervening GGG linker. No significant differences were observed between the immunogenicity of GPSL and GGG linker bearing P4 epitopes (Supporting figure 3).

The 30 nm icosahedral CPMV capsid and the 515 nm x 13 nm PVX filaments present ~300 and 1270 reactive lysine residues, respectively, enabling chemical conjugation with antigenic epitopes. A bi-functional *N*-hydroxysuccinimide-PEG4-maleimide (SM-PEG4) linker was used for coupling the C-terminal cysteine to the solvent-exposed lysine residues on either VNP (Figure 4B). SDS-gel electrophoresis of purified VNP-peptide formulations showed presence of additional higher molecular weight protein bands corresponding to modified coat protein subunits (Figure 4C). The small CP subunit of CPMV (S, 24 kDa) showed higher molecular weight bands corresponding to CH401- and P4 - modified S protein (lanes 2 and 3,

CPMV). Similar patterns were observed for PVX and its conjugated formulations PVX-CH401 and PVX-P4 (lanes 2 and 3, PVX). Densitometry analysis of the CP-peptide bands corresponding to CPMV-CH401 and CPMV-P4 (lanes 2 and 3 CPMV) indicated ~ 45±5% of small coat protein subunits were modified with the antigenic peptides, resulting in ~30 peptides per CPMV (it is likely that additional peptides are conjugated to the L protein, however the gel analysis did not allow us to quantify loading; mass spectrometry has been attempted with CPMV, but the L protein remains challenging to analyze due to its inherent insolubility when not assembled into a particle [77]. Similar analysis for PVX-P4 and PVX-CH401 (lanes 2 and 3 PVX) indicated ~24±3% coat proteins were modified corresponding to ~275 epitopes per PVX. With respect to the differences in molecular weights of the VNP formulations, peptide loading on PVX is about ~70% higher compared to CPMV attesting to higher payload delivery capabilities of the filamentous PVX platform.

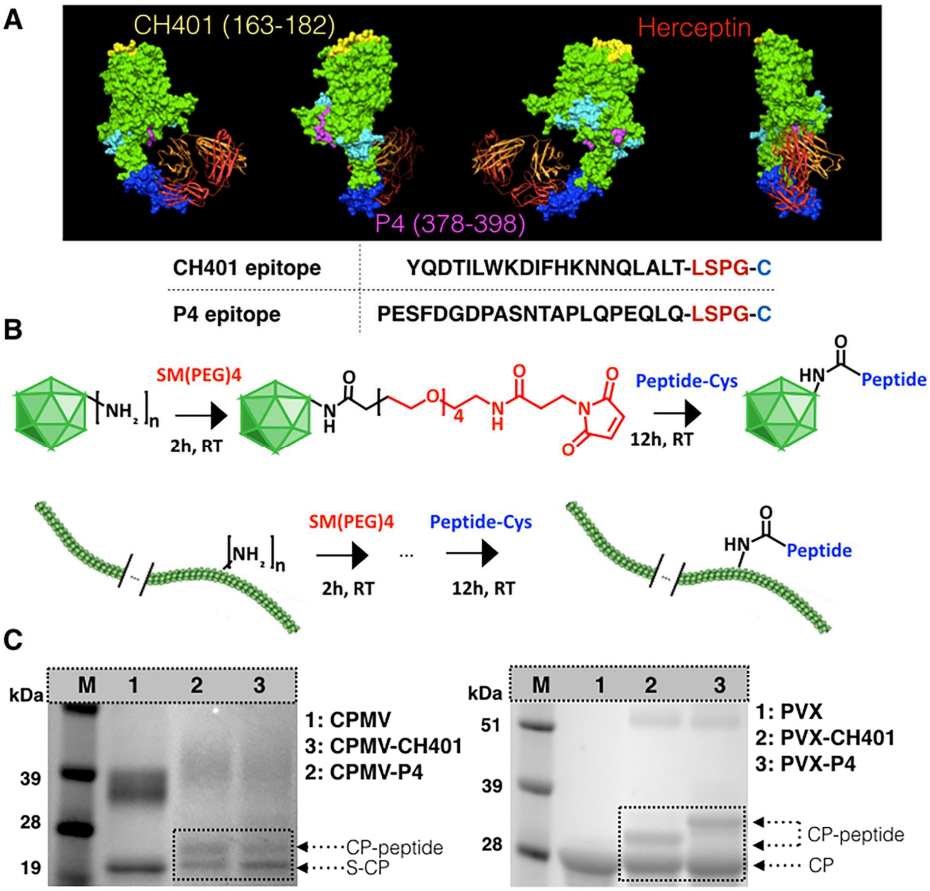

Figure 4. Design and synthesis of HER2 vaccine based on CPMV and PVX carriers. (A) Epitopes CH401 $_{(163\text{-}182)}$ and P4 $_{(378\text{-}398)}$ are derived from the distinct regions of the extracellular domain of HER2 different from Herceptin (Trastuzumab) binding domain. The epitopes were designed with a terminal Cysteine residue with an intervening flexible GPLS linker. (B) Epitopes were chemically conjugated to the reactive lysine residues on CPMV and PVX capsids in a two-step process via a bifunctional NHS-PEG4-MAL linker. (C) Denaturing SDS-gel electrophoresis analysis shows modification of CPMV and PVX capsid proteins with multiple copies of CH401 and P4 peptides resulting in appearance of additional high molecular weight bands corresponding peptide modified CPs.

Stimulation of HER2 peptide specific antibody responses: CPMV- and PVX-based HER2 vaccine formulations were evaluated for their ability to augment the serum antibody titers against the HER2 target. These studies were carried out by immunizing female FVB mice three times, biweekly with free peptide epitopes (CH401 or P4; 1.2 μg dose), 50 μg of peptide-loaded CPMV

or PVX (carrying 0.8 μg or 1.2 μg of peptides, respectively) (Figure 5A). Because previous studies had shown that the immunostimulatory and adjuvant properties of VNPs obviate the need for an external adjuvant [8, 78, 79], we chose not to use any adjuvants in our studies. After the initial set of immunizations (d0, d14 and d28), mice were boosted with similar doses of vaccine candidates on days 68, 81 and 96 (Figure 5A). Serum was collected prior to the first and all subsequent immunizations, and sera were analyzed for peptide epitope specific- and carrier-specific IgG levels using ELISAs at increasing dilutions (1:500, 1:2500 and 1:12500) (Figure 5B and 5C). The results illustrated a clear pattern: while the soluble peptides failed to stimulate significant levels of serum antibodies (black curves), multivalent arrays of the same epitopes on VNP carriers led to a strong peptide-specific IgG response. IgG levels peaked on day 28 following the second immunization on day 14; this pattern repeated upon booster administration, where the IgG levels peaked following the second booster on day 81. The antibody responses varied as a function of VNP carrier and choice of epitope. Overall, CPMV-based vaccine formulations (blue curves) triggered a considerably stronger HER2 peptide-specific immune response compared to the PVX-based vaccine formulations (red curves) (Figure 5B and 5C). These results corroborate enhanced trafficking and retention of CPMV particles to draining lymph nodes over PVX and increased uptake of CPMV by APCs, including DCs (Figure 2). Thus, CPMV particles as carriers are able to deliver the peptide epitopes to APCs more efficiently for processing and presentation, leading to the significantly high sera IgG levels over PVX vaccines.

Furthermore, differences were also observed comparing the different peptide formulations: CPMV-CH401 and PVX-CH401 vaccines led to elevated IgG levels over corresponding P4 epitope vaccines, suggesting enhanced immunogenicity of CH401 over P4

epitope (Figure 5B and 5C). Moreover, the CH401 vaccines (both CPMV and PVX based) resulted in sustained IgG levels between the peak days of d28 and d96, as compared to corresponding P4 vaccines where the IgG levels fall sharply in this period. Furthermore, booster immunization with CPMV vaccines resulted in elevated peptide specific IgG levels on day 96 (both anti-CH401 and anti-P4), however PVX vaccine boosters did not lead to enhanced IgG response with either epitope (Figure 5B). The alternative intervening linker GGG under consideration with P4 showed no significant difference in immunogenicity to P4 compared to the GPSL linker across all formulations except absence of elevated IgG response on d96 following booster administration with CPMV carriers (Supplementary figure S3). This could indicate inefficient processing of the GGG linker bearing P4, however, further studies will be needed to determine the mechanistic differences arising from peptide linkers.

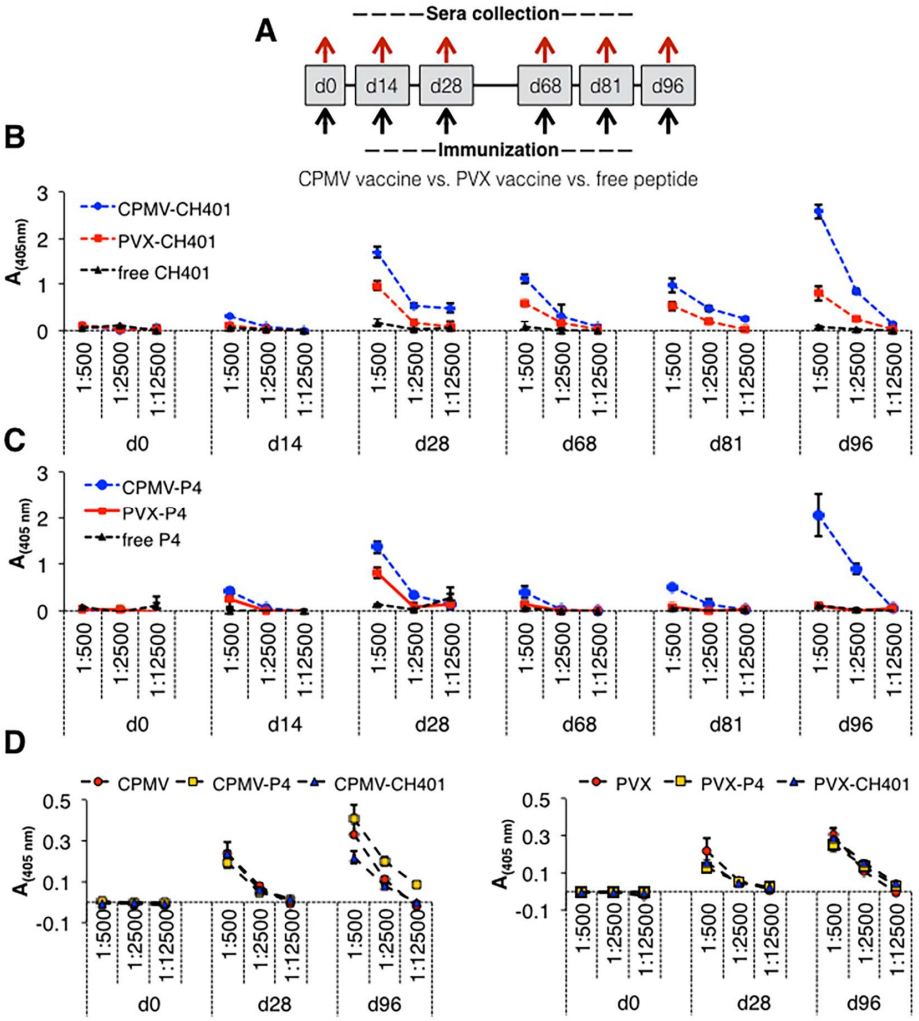

Figure 5. Characterization of antibody response to HER2 vaccines. (A) Immunization schedules with biweekly administration of VNP-based formulations or free peptides over a 96 day period. (B, C) ELISAs were performed to detect anti-CH401 and anti-P4 serum IgG levels (at 1: 500, 1:2500 and 1:12500 serum dilution) following immunization with CPMV vaccines (blue), PVX vaccines (red) or free peptides (black). **D)** Comparable carrier-specific IgG response was measured following immunization with CPMV and PVX or the vaccine formulations based on the two carrier VNPs.

The immunostimulatory nature of VNP carriers is critical and desirable for initiating a successful immune response directed against the epitopes. Self-tolerance and immunosuppression are often the biggest challenges in cancer vaccine-mediated

immunotherapies. It is therefore critical that a vaccine carrier provides the immunostimulatory impetus required for reactivating the immune system against tumor antigens by modulating antigen-immune cell interactions. However, immunogenicity of capsid proteins could result in a VNP-specific immune response at the cost of epitope-specific antibodies in a vaccine setting [80, 81]. Presence of carrier neutralizing antibodies may also lead to rapid clearance, lower bioavailability and potential systemic toxicities, resulting in undesirable off-target effects, and therefore is a major obstacle to success of VNP/VLP-based vectors and nanomedicinal platforms [21, 82, 83]. Therefore, we assessed the specificity of the IgG response toward HER2 epitopes vs. carrier VNPs. Sera from immunized mice were tested on plates coated with corresponding VNP (Figure 5D). Dilution series indicates that anti-VNP-specific IgGs were detectable at similar levels compared to anti-HER2 IgGs; however, the significantly lower absorbance indicates that the anti-VNP antibodies generated have lower affinity relative to the anti-HER2 antibodies. There were no differences between the humoral responses against the CPMV vs. PVX carrier.

In summary, these results highlight differences in the immunogenicity of the two HER2 epitopes, the influence of carrier VNP is clearly evident as well. Furthermore, the lack of humoral immune-stimulation using free peptides highlights the need of carrier. The data indicate that in the context of VNP presentation, the CH401 peptide is more potent compared to P4, and CH401 is most effective when presented as a multivalent array on the CPMV carrier (as opposed to PVX).

Differences in the vaccine efficiency of CPMV vs. PVX-based formulations may be attributed to the differential immunostimulatory nature of the two carriers, as a result of their distinct shape and molecular composition. CPMV with its natural tropism toward primary APCs,

may undergo APC- and macrophage-mediated uptake and antigen-processing resulting in more efficient immune stimulation involving T helper cells. PVX particles, on the other hand, avoid endocytosis and phagocytosis by APCs and macrophages and are sequestered in B cell rich regions, resulting in inefficient immune responses [59, 69]. Both, CPMV and PVX, have been previously studied as vaccine delivery platforms, demonstrating efficacy both to prime humoral and cellular responses [32-38]. Nevertheless, a direct comparison of the two platforms has not been reported.

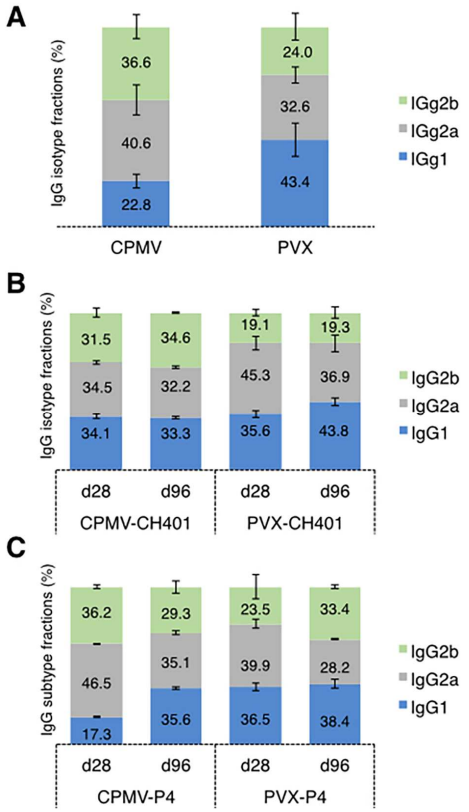

Figure 6. IgG Isotyping. ELISA measurements were used to determine VNP-specific (A) and epitope-specific (B & C) IgG isotypes in immunized mice sera. Isotype breakdown is shown as IgG1/IgG2a/IgG2b fractions (representative data are shown with mean and standard deviation from 3 technical replica).

IgG isotyping was performed to further characterize the nature of the immune response to carriers and vaccines. CPMV-immunized mice showed significantly higher levels of anti-CPMV IgG2a/2b isotypes levels over IgG1 isotypes (40.6% and 36.6% vs. 22.8%, respectively), whereas PVX immunized mice showed an anti-PVX IgG response skewed toward IgG1 isotype (43%) over IgG2a/2b (36/19%, respectively) (Figure 6A). The differences between IgG isotype suggest distinct immunostimulatory properties of CPMV and PVX particles and that could, in part, arise from their differential trafficking, interactions with immune system components, or engagement of distinct TLR receptors. While all the IgG variant bind to Fc receptors and can enhance phagocytosis by macrophages, each isotype can confer specific therapeutic advantage. Therefore, while IgG1 can fix complement and mediate antibody dependent cell cytotoxicity (ADCC) of cancer cells by natural killer cells [84], mouse IgG1 is considered a low effector function isotype, whereas IgG2a/2b have the highest binding affinities to FcγRs and are particularly potent mediator of ADCC by myeloid cells including neutrophils [85, 86]. The carrier immunogenicity seems to influence epitope specific IgG isotype profiles of the two HER2 vaccines, although the two epitopes also had an impact. CH401-specific IgG showed a broader isotype profile when presented on CPMV (IgG1/IgG2a/IgG2b fractions of 34/34/31%) as compared to CH401 displayed on PVX (IgG1/IgG2a/IgG2b fractions of 35/45/19%) (Figure 6B). The breakdown of P4-specific IgG response on day 28 showed characteristic isotype profiles mirroring CPMV and PVX-specific IgG responses skewed toward IgG2a and IgG2b vs. IgG1, respectively (Figure 6C). However, at day 96, P4-specific isotypes for both CPMV and PVX based vaccines are not significantly different (Figure 6C).

Anti-sera recognition of cellular HER2 receptor: Next, we determined the whether serum IgGs toward the target antigen HER2 target the cellular receptor; flow cytometry and confocal

microscopy studies using SKBR3 cells were performed as well as ELISA analysis against recombinant HER2 protein (Figure 7).

SKBR3 cells were incubated with pooled antisera from various immunization groups and analyzed by flow cytometry (Figure 7A). A commercial anti-HER2 IgG was used as a positive control, whereas serum from naïve mice and commercially procured mouse total IgG were used as negative controls. Total IgG from naïve mice showed minimal binding, indicating absence of non-specific HER2 affinity in mouse sera. Antisera from CPMV and PVX vaccine immunized mice showed variable positive interactions with SKBR3 cells with CPMV-CH401 antisera showing significantly higher binding over CPMV-P4 antisera and all PVX-based formulations. Increased interaction of CPMV-CH401 antisera over CPMV-P4 sera could reflect higher titers of HER2 specific antibody in the former over latter, underlining the higher immunogenicity of CH401 peptide over P4 peptide. Moreover, the highly exposed CH401 domain on the HER2 extracellular domain is likely to contribute towards improved binding of CH401 antisera over P4 antisera for both CPMV and PVX. This differential binding affinity with cellular HER2 receptor was further validated by confocal microscopy where CPMV-CH401 antisera clearly showed enhanced binding with membrane HER2 (Figure 7C) (comparable to anti-HER2 antibody, Figure 7B) over PVX-CH401 antisera when inoculated with SKBR3 cells (Figure 7D). Furthermore, differential binding of CPMV-CH401 antisera or its PVX counterpart with HER2 was also confirmed using ELISA, where the former showed ~1.5 times higher binding with HER2 protein over the latter (Figure 7E). These results clearly highlight the ability of CPMV-based HER2 vaccines to stimulate a stronger and specific immune response against HER2.

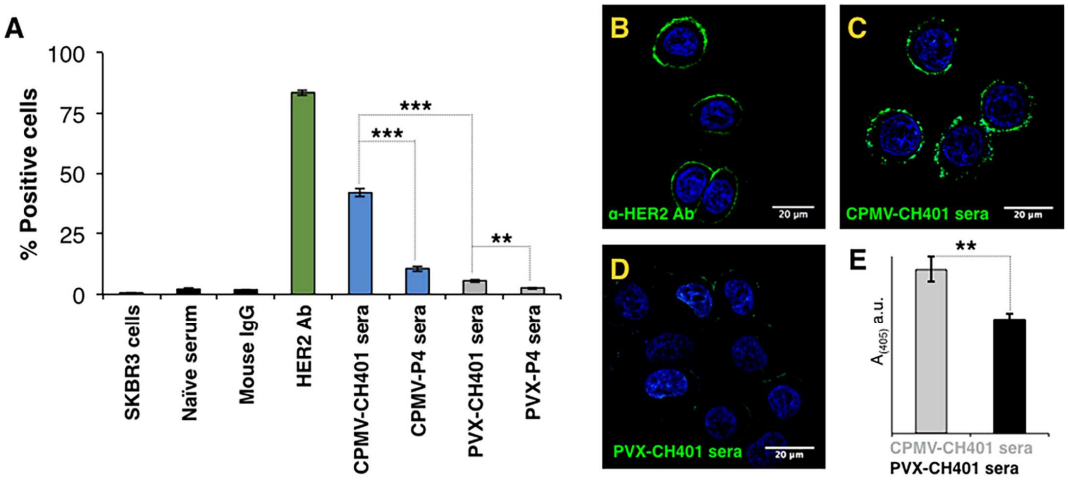

Figure 7. Specificity of serum IgGs toward cellular HER2 receptors. (A) Flow cytometry analysis comparing serum IgG binding with HER2+ SKBR3 cells. (B-D) Confocal analysis comparing the binding of vaccine stimulated serum IgGs (by CPMV-CH401 and PVX-CH401) and anti-HER2 antibody to cellular HER2 receptors on SKBR3 cells. (E) ELISA comparing binding of serum IgGs to recombinant HER2 protein. Student T test was used for statistical analysis with ** = $p<0.01$ and *** = $p< 0.001$.

Conclusions:

Cancer vaccines can activate the immune system to recognize tumor-associated antigens and have the potential to eliminate residual or retuning tumors following primary treatment via antigen specific cellular or humoral responses. An effective cancer vaccine combines immunodominant epitopes with efficient delivery vehicles, thereby optimizing interactions with components of the immune system including secondary lymphoid tissues and antigen presenting cells. Plant VNPs with highly organized multivalent architectures and natural tropism for immune cells are therefore ideally suited for this role. Based on their structural differences, VNPs may engage distinct cellular populations and initiate alternative pathways influencing the extent and type of immune response to carrier epitopes. This study highlights the underlying differences between *in vivo* trafficking and cellular interactions that renders one VNP more

potent than another. Data indicate CPMV is superior for displaying B cell epitopes and stimulating an epitope-specific humoral response (with minimal development of carrier-specific antibodies). *In vivo* trafficking of PVX deep into the B cell follicles in dLNs may open novel applications targeting these immune cell reservoirs. Our studies highlight the need for systematic analysis of VNP carriers to define rules guiding the design, and rationale choice of platform, in the context of peptide-vaccine display technologies.

Materials and Methods:

VNP propagation: Established procedures were used for the propagation and purification of CPMV [87] and PVX [20]. Purified VNPs were stored in 0.1 M potassium phosphate pH 7.0 buffer at 4°C. Concentrations of VNPs were determined by UV spectroscopy at 260 nm using the molar extinction coefficients ε_{CPMV} = 8.1 mL mg^{-1} cm^{-1} and ε_{PVX}= 2.97 mL mg^{-1} cm^{-1}.

Synthesis of CPMV and PVX vaccine formulations: HER2 epitopes P4 $_{(378-398)}$ and CH401 $_{(163-182)}$ were conjugated to purified CPMV and PVX VNPs using NHS chemistry. In a two-step protocol, cysteine terminated peptide epitopes P4 (PESFDGDPASNTAPLQPEQLQ-LSPG-**C**) and CH401 (YQDTILWKDIFHKNNQLALT-LSPG-**C**) with flexible GPSL linker [76] were conjugated to VNPs via the heterobifunctional *N*-hydroxysuccinimide-PEG_4-maleimide linker SM-PEG4 (Life Technologies). The peptides were synthesized and obtained from Genscript. Briefly, CPMV and PVX were reacted with 3500 and 5000 molar excess of SM-PEG4 linker at room temperature for 2 h at a 2 mg mL^{-1} VNP concentration. Then, 5000 and 7500 molar excess of peptides were reacted overnight with SM-PEG4-modified CPMV and PVX, respectively. VNP-peptide formulations were purified over a 40% (w/v) sucrose cushion at 160,000 x g for 3 h and resuspended in sterile PBS. UV spectroscopy was used to determine VNP concentrations as described above and the peptide conjugation was quantified using lane density analysis (ImageJ 1.44o software (http://imagej.nih.gov/ij) of protein bands following SDS gel electrophoresis.

Synthesis of fluorescently tagged VNPs. CPMV and PVX VNPs were covalently modified with AlexaFluor 647 (A647) dye using *N*-hydroxysuccinimide-activated esters targeting surface-exposed lysine residues on the viral coat proteins (NHS-A647 was obtained from Life Technologies). CPMV and PVX were incubated overnight at room temperature with 3500 and 5000 molar excess of NHS-A647, respectively. CPMV-A647 and PVX-A647 were then purified

using ultracentrifugation on a 40% (w/v) sucrose cushion. UV-Vis spectroscopy performed on a Nanodrop instrument was used to determine A647/ VNP ratio using fluorophore-specific extinction coefficients of ε_{A647} = 270,000 $M^{-1}cm^{-1}$ at 650 nm, ε_{CPMV} = 8.1 mL mg^{-1} cm^{-1} at 260 and ε_{PVX} = 2.97 mL $mg^{-1}cm^{-1}$ at 260 nm.

Immunization: All experiments were carried out in accordance with Case Western Reserve University's Institutional Animal Care and Use Committee. Female FVB mice (n=3) were immunized subcutaneously on days 0, 14 and 28 with formulations consisting of 50 μg of VNP-peptide conjugates (CPMV-P4/ CH401 or PVX-P4/ CH401 with CPMV carrying 0.8 μg peptide load and PVX carrying 1.2 μg peptide load) or equivalent amounts of free peptides (P4 or CH401) or VNP carriers (CPMV and PVX) suspended in 50 μL PBS, followed by a course of biweekly booster immunization with these same (on days 68, 81 and 96). Blood was collected prior to every immunization (days 0, 14, 28, 68, 81 and 96) and 2 weeks after the last booster injection (on day 110) through the retro-orbital plexus. Blood was collected in Greiner Bio-One VACUETTE™ MiniCollect™ tubes (Thermo Fisher Scientific, Waltham, MA) and centrifuged at 14,800 rpm for 10 min to separate the serum, which was then stored at 4°C until analyzed. All mice were euthanized after the last blood collection.

Enzyme-linked immunosorbent assays (ELISAs): Following immunizations, ELISAs were carried out to determine levels of epitope and VNP-specific serum IgG and IgG isotypes as well as HER2 specific IgG. Peptide-specific ELISA was performed on the 96-well Pierce™ Maleimide Activated Plates (Thermo Fisher Scientific) prepared and processed as per manufacturer's instructions. Briefly, plates were coated with 0.4 μg of peptide (P4, $P4_{ii}$, or CH401) per well in coating buffer (0.1M sodium phosphate, 0.15 M sodium chloride, 10 mM EDTA, pH 7.2) and incubated overnight at 4°C. Following blocking with 100 μL cysteine

solution (10 µg/mL) per well at 37°C for 1 hour, sera from immunized mice at dilutions of,1:500, 1:2500 and 1:12500 (in coating buffer) were added to the wells and incubated at 37°C for 2 h. Plates were washed four times with washing buffer (0.05% (v/v) Tween-20 in PBS, 200 µL per well) between all steps. Plates were then incubated with 100 µL of alkaline phosphatase-labeled goat anti-mouse IgG (Invitrogen, Thermo Fisher Scientific) in blocking buffer (at 1:3000 dilution) at 37°C for 1 hour and developed with 100 µL of 1-step PNPP substrate (Thermo Fisher Scientific) for 10 min at 4°C. Reaction was stopped using 50 µL of 2 M NaOH. Absorbance was then read at 405 nm using a Tecan microplate reader. IgG isotyping was similarly carried out using anti-mouse IgG2a, IgG2b and IgG1-alkaline phosphatase antibodies (Novus Biologicals, Littleton, CO) at 1:1000 dilutions. VNP-specific IgG and isotypes levels were similarly determined on a 96-well Nunc Polysorp Immuno plates (Thermo Fisher Scientific) coated with 1 µg of VNPs (CPMV or PVX). HER2 specific serum IgG levels were determined using plates coated with 1 µg human HER2/ ErbB2 protein (Acro Biosystems, Newark , DE).

Cell Binding Assay: $HER2^+$ SK-BR-3 cells (ATCC) were maintained in McCoy's 5A media supplemented with 10% (v/v) fetal bovine serum and 1% (v/v) Penicillin/Streptomycin (all reagents from Life Technologies, Grand Island, NY) at 37°C and 5% CO_2. For the cell-binding assay, 25,000 SK-BR-3 cells per well were cultured on glass coverslips in a 24-well suspension culture plate for 24 h. After washing and replacing with fresh media, pooled antisera from mice immunized with CPMV- and PVX-based vaccines were added to the culture media (1:500 dilution) and incubated with cells at at 4°C for 2 h. A rabbit anti-human HER2 Ab (ACRO Biosystems, Newark, DE) was used as a positive control. Post-incubation, cells were washed thrice with sterile saline and fixed for 5 min at room temperature with DPBS containing 4% (v/v) paraformaldehyde and 0.3% (v/v) glutaraldehyde. Antisera treated cells were stained with goat

anti-mouse-AlexaFluor 488 secondary antibody (1:1000 dilution; Life Technologies) in 5% (v/v) goat serum. HER2 antibody treated cells were stained with goat anti-rabbit AlexaFluor 488 secondary antibody (1:1000) (Life Technologies) for 60 min at room temperature. Cells were washed thrice with DPBS (Life Technologies). All coverslips were then mounted onto glass slides using Fluoroshield with DAPI mounting media (Sigma, St. Louis, MO) resulting in nuclear staining and sealed using nail polish. Confocal images were captured on an Olympus FluoViewTM FV1000 LSCM and data processed using ImageJ 1.44o software (http://imagej.nih.gov/ij).

Flow cytometry: SKBR3 cells were cultured as described above. The cells were washed with PBS, collected in enzyme-free Hank's-based Cell Dissociation Buffer (Fisher), and re-suspended in 200 µL of complete medium in a 96 well plate at 200,000 cells/ well. Cells were then incubated for 2 h at 4°C with rabbit anti-HER2 Ab (1:500 dilution), mouse total IgG (1:500 dilution), sera from naïve mice, and sera from mice immunized with CPMV vaccines (CH401 and P4) and sera from mice immunized with PVX vaccines (CH401 and P4). Post-incubation, cells were washed twice in FACS buffer (1 mM EDTA, 25 mM HEPES, 1% (v/v) FBS in PBS, pH 7.0), fixed in 2% (v/v) paraformaldehyde in FACS buffer for 10 min at room temperature and washed twice again in FACS buffer. Antisera treated and mouse total IgG treated cells were then stained with goat anti-mouse IgG antibody conjugated with AlexaFluor 488 (1: 1000 dilution) whereas cells incubated with rabbit anti-HER2 antibody were stained with Cells were then stained with goat anti-rabbit Alexa Fluor 488 secondary antibody (1:1000) (Life Technologies) for 60 min at 4°C. Cells were then washed twice in FACS buffer, re-suspended in 300 µL FACS buffer, and stored at 4°C. Cells were analyzed using a BD LSR II Flow Cytometer and 10,000 gated events were recorded. Data were analyzed using FlowJo v8.6.3 software.

Bone marrow derived dendritic cells (BMDCs) uptake and cytokine activation: BMDC were obtained according to previously published protocols [45]. Briefly, a single cell suspension of whole bone marrow cells was obtained from the femurs and tibias of female FVB mice. The cells were washed once in PBS and red cells were lysed for 2 minutes at 37^{o}C in 2 ml of ACK lysis solution (Lonza, Allendale, NJ). The cells were filtered, washed, and resuspended at 1x10^{6} cells/ml in T cell media (RPMI (Corning, Croning, NY) supplemented with 10% GemCell FBS (Gemini Bio-Products, Sacramento, CA), 1x penicillin/streptomycin (Corning), 1x MEM non-essential amino acids (Corning), 1 mM sodium pyruvate (HyClone, South Logan, UT), 2 mM L-glutamine (Corning), 10 mM HEPES (Corning), and 50 µM beta-mercaptoethanol (Sigma)) supplemented with 10 ng/ml mouse IL-4 (Peprotech, Rocky Hill, NJ) and 15 ng/mL mouse GM-CSF (Peprotech). 3 mL of cells were plated/well of a 6-well plate and incubated at 37^{o}C. The media was removed and replaced with fresh T cell media supplemented with IL-4 and GM-CSF on day 3 and an additional 3 mL of fresh T cell media supplemented with cytokines was added on day 5. Cells were harvested on day 7 and used for VNP uptake and cytokine activation studies. All cells were maintained on ice prior to the addition of VNPs. For BMDC uptake studies, A647-CPMV and A647-PVX particles (at 50,000 particles/ cell) were incubated with 1 x 10^{6} cells at 37^{o}C for 2 h. Cells were washed to remove free particles and incubated with 100 µl of Fc Block (1:400, anti-CD16/32, eBioscience, San Diego, CA) on ice for 20 minutes to block Fc receptor-mediated non-specific interactions. Following this, cells were stained with PE-anti-CD11c (1:100, BioLegend, San Diego, CA) for 30 minutes on ice. Samples were analyzed on a BD Accuri cytometer.

For cytokine activation assay, BMDCs were incubated with CPMV and PVX particles (5 µg VNPs/ million cells) at 37 ^{o}C for 24 h in cytokine free T cell media. Bacterial LPS at 100 ng/mL

was used as a positive control. Following incubation, cell supernatants were collected and aliquot were stored at -20 ^{o}C until analyzed by ELISAs (ELISA MAX TM Standard, Biolegend) for TNF-α and IL-6.

Lymph node trafficking and uptake by antigen presenting cells (APCs). Draining lymph node (dLN) homing of VNP carriers was studied using the fluorescently tagged CPMV and PVX particles (A647-CPMV and A647-PVX, respectively). First, to observe the differential trafficking of CPMV and PVX, female FVB/N mice were subcutaneously injected with 50 μg (in 20 μL PBS) each of CPMV-A647 and PVX-A647 in left and right footpad, respectively. Maestro imaging system (Perkin Elmer) was then used to monitor accumulation of fluorescent signals in the corresponding popliteal lymph nodes over time. To determine the draining lymph node in vaccine setting, female FVB/N mice were subjected to a single sub-cutaneous administration of 100 μg VNPs (in 100 μL PBS) behind the neck. Mice were sacrificed at 12 h, 24 h and 48 h post injections and the resected draining LNs (brachial) were imaged for total fluorescence using Maestro imaging system and/or digested into a single cell suspension for analysis of VNP distribution in various cell types by flow cytometry. Draining lymph nodes (dLNs) were harvested, sliced in half and digested with 0.2 mg/ml collagenase D (Sigma) and 200 units DNase-1 (Sigma) for 30 minutes at 37^{o}C and then passed through a 40 μm cell strainer to prepare a single cell suspension in FACS buffer. Cells were then treated with anti-CD16/32 Fc block (eBiosciences) on ice for 20 minutes and then stained with anti-CD19-FITC (eBioscience), anti-CD11c-PE (BioLegend), or anti-F4/80-PE (BioLegend) for 35 minutes on ice. In order to determine the activation status CD11c^{+} dendritic cells and F4/80^{+} macrophages in the DLNs of VNP injected mice, some cells from 24 hr injected LNs were additionally prepared as above and stained for 45 minutes on ice with anti-CD11c-biotin (BD Biosciences) in conjunction with

either anti-CD86-PE (eBioscience) or anti-CD40-PE (BD Biosciences) followed by a secondary staining with Streptavadin-FITC (eBioscience) for 20 minutes on ice. Additionally, some cells were stained with anti-F4/80-FITC (BioLegend) along with either anti-CD86-PE or anti-CD206-PE (BioLegend) for 45 minutes on ice. 7-AAD (eBioscience) was also used for live-dead cell discrimination. The samples were run on a BD Accuri cytometer for analysis. For IHC analysis, draining lymph nodes were harvested 12 h after injecting mice with A647-CPMV or A647-PVX particles, fixed overnight in PLP, and then incubated for 24 hrs in sterile 30% sucrose solution at 4^{o}C. dLNs were then embedded in OCT and cryosectioned. LN sections were then stained with purified rat anti-mouse B220 antibody (BD Pharmingen) followed by AF488-goat anti-rat secondary (ThermoFisher) using a Pelco Biowave (Ted Pella, Inc. city ST) and imaged on a Olympus Fluoview 1000 microscope.

Acknowledgements:

This work was supported in parts by a grant from the Susan G. Komen foundation (CCR14298962 to N Steinmetz) and National Science Foundation REU supplement under award CMMI-1333651 (to NSF). A. Wen is acknowledged for TEM imaging of VNPs. F. Allen is acknowledged for assisting with BMDC isolation and dLN processing protocols and discussions. S. Eid is acknowledged for assistance with cryo-sectioning lymph nodes.

Supplementary material: Cytokine activation measurements following VNP incubation with BMDCs (Supplementary figure 1), Immunofluorescence imaging of dLN harvested 24 h following subcutaneous A647-PVX injection (Supplementary figure 2) and ELISA measurements comparing immunogenicity of P4 peptide (with GPSL linker) and P4(ii) peptide (with GGG linker) (Supplementary figure 3).

References:

[1] Pilla L, Rivoltini L, Patuzzo R, Marrari A, Valdagni R, Parmiani G. Multipeptide vaccination in cancer patients. Expert Opin Biol Ther. 2009;9:1043-55.
[2] Azvolinsky A. Cancer vaccines: always a bridesmaid, never a bride? J Natl Cancer Inst. 2013;105:248-9.
[3] Winter H, Fox BA, Ruttinger D. Future of cancer vaccines. Methods Mol Biol. 2014;1139:555-64.
[4] Weber JS, Yang JC, Atkins MB, Disis ML. Toxicities of Immunotherapy for the Practitioner. J Clin Oncol. 2015;33:2092-9.
[5] Alatrash G, Jakher H, Stafford PD, Mittendorf EA. Cancer immunotherapies, their safety and toxicity. Expert opinion on drug safety. 2013;12:631-45.
[6] Melero I, Gaudernack G, Gerritsen W, Huber C, Parmiani G, Scholl S, et al. Therapeutic vaccines for cancer: an overview of clinical trials. Nat Rev Clin Oncol. 2014;11:509-24.
[7] Bolhassani A, Safaiyan S, Rafati S. Improvement of different vaccine delivery systems for cancer therapy. Mol Cancer. 2011;10:3.
[8] Krishnamachari Y, Geary SM, Lemke CD, Salem AK. Nanoparticle delivery systems in cancer vaccines. Pharm Res. 2011;28:215-36.
[9] Fan Y, Moon JJ. Nanoparticle Drug Delivery Systems Designed to Improve Cancer Vaccines and Immunotherapy. Vaccines (Basel). 2015;3:662-85.
[10] Shukla S, Steinmetz NF. Emerging nanotechnologies for cancer immunotherapy. Exp Biol Med (Maywood). 2016;241:1116-26.
[11] Goldberg MS. Immunoengineering: how nanotechnology can enhance cancer immunotherapy. Cell. 2015;161:201-4.
[12] van der Veen AH, Eggermont AM, Seynhaeve AL, van T, ten Hagen TL. Biodistribution and tumor localization of stealth liposomal tumor necrosis factor-alpha in soft tissue sarcoma bearing rats. Int J Cancer. 1998;77:901-6.
[13] Park J, Wrzesinski SH, Stern E, Look M, Criscione J, Ragheb R, et al. Combination delivery of TGF-beta inhibitor and IL-2 by nanoscale liposomal polymeric gels enhances tumour immunotherapy. Nat Mater. 2012;11:895-905.
[14] Anderson PM, Katsanis E, Sencer SF, Hasz D, Ochoa AC, Bostrom B. Depot characteristics and biodistribution of interleukin-2 liposomes: importance of route of administration. J Immunother (1991). 1992;12:19-31.
[15] Sheng WY, Huang L. Cancer immunotherapy and nanomedicine. Pharmaceutical research. 2011;28:200-14.
[16] Steinmetz NF. Viral nanoparticles as platforms for next-generation therapeutics and imaging devices. Nanomedicine. 2010;6:634-41.
[17] Plummer EM, Manchester M. Viral nanoparticles and virus-like particles: platforms for contemporary vaccine design. Wiley Interdiscip Rev Nanomed Nanobiotechnol. 2010.
[18] Lee KL, Twyman RM, Fiering S, Steinmetz NF. Virus-based nanoparticles as platform technologies for modern vaccines. Wiley Interdiscip Rev Nanomed Nanobiotechnol. 2016.
[19] Pokorski JK, Steinmetz NF. The art of engineering viral nanoparticles. Molecular pharmaceutics. 2011;8:29-43.
[20] Shukla S, Wen AM, Ayat NR, Commandeur U, Gopalkrishnan R, Broome AM, et al. Biodistribution and clearance of a filamentous plant virus in healthy and tumor-bearing mice. Nanomedicine (Lond). 2014;9:221-35.

[21] Yildiz I, Shukla S, Steinmetz NF. Applications of viral nanoparticles in medicine. Current opinion in biotechnology. 2011;22:901-8.
[22] Garcia Casado J, Janda J, Wei J, Chapatte L, Colombetti S, Alves P, et al. Lentivector immunization induces tumor antigen-specific B and T cell responses in vivo. Eur J Immunol. 2008;38:1867-76.
[23] Odunsi K, Qian F, Matsuzaki J, Mhawech-Fauceglia P, Andrews C, Hoffman EW, et al. Vaccination with an NY-ESO-1 peptide of HLA class I/II specificities induces integrated humoral and T cell responses in ovarian cancer. Proc Natl Acad Sci U S A. 2007;104:12837-42.
[24] Odunsi K, Matsuzaki J, Karbach J, Neumann A, Mhawech-Fauceglia P, Miller A, et al. Efficacy of vaccination with recombinant vaccinia and fowlpox vectors expressing NY-ESO-1 antigen in ovarian cancer and melanoma patients. Proc Natl Acad Sci U S A. 2012;109:5797-802.
[25] Breckpot K, Aerts JL, Thielemans K. Lentiviral vectors for cancer immunotherapy: transforming infectious particles into therapeutics. Gene Ther. 2007;14:847-62.
[26] Wen AM, Le N, Zhou X, Steinmetz NF, Popkin DL. Tropism of CPMV to Professional Antigen Presenting Cells Enables a Platform to Eliminate Chronic Infections. Acs Biomater-Sci Eng. 2015;1:1050-4.
[27] Christian DA, Hunter CA. Particle-mediated delivery of cytokines for immunotherapy. Immunotherapy. 2012;4:425-41.
[28] Lizotte PH, Wen AM, Sheen MR, Fields J, Rojanasopondist P, Steinmetz NF, et al. In situ vaccination with cowpea mosaic virus nanoparticles suppresses metastatic cancer. Nat Nanotechnol. 2015.
[29] Shukla S, Eber FJ, Nagarajan AS, DiFranco NA, Schmidt N, Wen AM, et al. The Impact of Aspect Ratio on the Biodistribution and Tumor Homing of Rigid Soft-Matter Nanorods. Adv Healthc Mater. 2015;4:874-82.
[30] Shukla S, Ablack AL, Wen AM, Lee KL, Lewis JD, Steinmetz NF. Increased tumor homing and tissue penetration of the filamentous plant viral nanoparticle Potato virus X. Molecular pharmaceutics. 2013;10:33-42.
[31] Lee KL, Shukla S, Wu M, Ayat NR, El Sanadi CE, Wen AM, et al. Stealth filaments: Polymer chain length and conformation affect the in vivo fate of PEGylated potato virus X. Acta Biomater. 2015;19:166-79.
[32] Lizotte PH, Wen AM, Sheen MR, Fields J, Rojanasopondist P, Steinmetz NF, et al. In situ vaccination with cowpea mosaic virus nanoparticles suppresses metastatic cancer. Nat Nanotechnol. 2016;11:295-303.
[33] Uhde-Holzem K, Schlosser V, Viazov S, Fischer R, Commandeur U. Immunogenic properties of chimeric potato virus X particles displaying the hepatitis C virus hypervariable region I peptide R9. J Virol Methods. 2010;166:12-20.
[34] Shukla S, Wen AM, Commandeur U, Steinmetz NF. Presentation of HER2 epitopes using a filamentous plant virus-based vaccination platform. J Mater Chem B. 2014;2:6249-58.
[35] Marusic C, Rizza P, Lattanzi L, Mancini C, Spada M, Belardelli F, et al. Chimeric plant virus particles as immunogens for inducing murine and human immune responses against human immunodeficiency virus type 1. J Virol. 2001;75:8434-9.
[36] Mardanova ES, Kotlyarov RY, Kuprianov VV, Stepanova LA, Tsybalova LM, Lomonosoff GP, et al. Rapid high-yield expression of a candidate influenza vaccine based on the

ectodomain of M2 protein linked to flagellin in plants using viral vectors. BMC Biotechnol. 2015;15:42.
[37] Lico C, Mancini C, Italiani P, Betti C, Boraschi D, Benvenuto E, et al. Plant-produced potato virus X chimeric particles displaying an influenza virus-derived peptide activate specific CD8+ T cells in mice. Vaccine. 2009;27:5069-76.
[38] Jobsri J, Allen A, Rajagopal D, Shipton M, Kanyuka K, Lomonossoff GP, et al. Plant virus particles carrying tumour antigen activate TLR7 and Induce high levels of protective antibody. PloS one. 2015;10:e0118096.
[39] Ross JS, Fletcher JA. The HER-2/neu Oncogene in Breast Cancer: Prognostic Factor, Predictive Factor, and Target for Therapy. Oncologist. 1998;3:237-52.
[40] Cho HS, Mason K, Ramyar KX, Stanley AM, Gabelli SB, Denney DW, Jr., et al. Structure of the extracellular region of HER2 alone and in complex with the Herceptin Fab. Nature. 2003;421:756-60.
[41] Sachdev JC, Jahanzeb M. Blockade of the HER family of receptors in the treatment of HER2-positive metastatic breast cancer. Clin Breast Cancer. 2012;12:19-29.
[42] Ladjemi MZ, Jacot W, Chardes T, Pelegrin A, Navarro-Teulon I. Anti-HER2 vaccines: new prospects for breast cancer therapy. Cancer Immunol Immunother. 2010;59:1295-312.
[43] Dakappagari NK, Lute KD, Rawale S, Steele JT, Allen SD, Phillips G, et al. Conformational HER-2/neu B-cell epitope peptide vaccine designed to incorporate two native disulfide bonds enhances tumor cell binding and antitumor activities. J Biol Chem. 2005;280:54-63.
[44] Baxevanis CN, Sotiropoulou PA, Sotiriadou NN, Papamichail M. Immunobiology of HER-2/neu oncoprotein and its potential application in cancer immunotherapy. Cancer Immunol Immunother. 2004;53:166-75.
[45] Antonopoulos C, Russo HM, El Sanadi C, Martin BN, Li X, Kaiser WJ, et al. Caspase-8 as an Effector and Regulator of NLRP3 Inflammasome Signaling. J Biol Chem. 2015;290:20167-84.
[46] Cervantes-Barragan L, Zust R, Maier R, Sierro S, Janda J, Levy F, et al. Dendritic cell-specific antigen delivery by coronavirus vaccine vectors induces long-lasting protective antiviral and antitumor immunity. MBio. 2010;1.
[47] Bachmann MF, Jennings GT. Vaccine delivery: a matter of size, geometry, kinetics and molecular patterns. Nature reviews Immunology. 2010;10:787-96.
[48] Fang RH, Kroll AV, Zhang L. Nanoparticle-Based Manipulation of Antigen-Presenting Cells for Cancer Immunotherapy. Small. 2015;11:5483-96.
[49] Ahsan F, Rivas IP, Khan MA, Torres Suarez AI. Targeting to macrophages: role of physicochemical properties of particulate carriers--liposomes and microspheres--on the phagocytosis by macrophages. J Control Release. 2002;79:29-40.
[50] Hardy CL, Lemasurier JS, Mohamud R, Yao J, Xiang SD, Rolland JM, et al. Differential uptake of nanoparticles and microparticles by pulmonary APC subsets induces discrete immunological imprints. J Immunol. 2013;191:5278-90.
[51] Irvine DJ, Swartz MA, Szeto GL. Engineering synthetic vaccines using cues from natural immunity. Nat Mater. 2013;12:978-90.
[52] Gallucci S, Matzinger P. Danger signals: SOS to the immune system. Curr Opin Immunol. 2001;13:114-9.

[53] Matzinger P. Tolerance, danger, and the extended family. Annu Rev Immunol. 1994;12:991-1045.
[54] Albanese A, Tang PS, Chan WC. The effect of nanoparticle size, shape, and surface chemistry on biological systems. Annu Rev Biomed Eng. 2012;14:1-16.
[55] Petros RA, DeSimone JM. Strategies in the design of nanoparticles for therapeutic applications. Nat Rev Drug Discov. 2010;9:615-27.
[56] Gonzalez MJ, Plummer EM, Rae CS, Manchester M. Interaction of Cowpea mosaic virus (CPMV) nanoparticles with antigen presenting cells in vitro and in vivo. PloS one. 2009;4:e7981.
[57] Koudelka KJ, Destito G, Plummer EM, Trauger SA, Siuzdak G, Manchester M. Endothelial targeting of cowpea mosaic virus (CPMV) via surface vimentin. PLoS Pathog. 2009;5:e1000417.
[58] Steinmetz NF, Cho CF, Ablack A, Lewis JD, Manchester M. Cowpea mosaic virus nanoparticles target surface vimentin on cancer cells. Nanomedicine (Lond). 2011;6:351-64.
[59] Mueller SN, Tian S, DeSimone JM. Rapid and Persistent Delivery of Antigen by Lymph Node Targeting PRINT Nanoparticle Vaccine Carrier To Promote Humoral Immunity. Molecular pharmaceutics. 2015;12:1356-65.
[60] Manolova V, Flace A, Bauer M, Schwarz K, Saudan P, Bachmann MF. Nanoparticles target distinct dendritic cell populations according to their size. Eur J Immunol. 2008;38:1404-13.
[61] Reddy ST, Rehor A, Schmoekel HG, Hubbell JA, Swartz MA. In vivo targeting of dendritic cells in lymph nodes with poly(propylene sulfide) nanoparticles. J Control Release. 2006;112:26-34.
[62] Kourtis IC, Hirosue S, de Titta A, Kontos S, Stegmann T, Hubbell JA, et al. Peripherally administered nanoparticles target monocytic myeloid cells, secondary lymphoid organs and tumors in mice. PloS one. 2013;8:e61646.
[63] Dukhin SS, Labib ME. Convective diffusion of nanoparticles from the epithelial barrier toward regional lymph nodes. Adv Colloid Interface Sci. 2013;199-200:23-43.
[64] Al Kobiasi M, Chua BY, Tonkin D, Jackson DC, Mainwaring DE. Control of size dispersity of chitosan biopolymer microparticles and nanoparticles to influence vaccine trafficking and cell uptake. J Biomed Mater Res A. 2012;100:1859-67.
[65] Carrasco YR, Batista FD. B cells acquire particulate antigen in a macrophage-rich area at the boundary between the follicle and the subcapsular sinus of the lymph node. Immunity. 2007;27:160-71.
[66] Phan TG, Gray EE, Cyster JG. The microanatomy of B cell activation. Curr Opin Immunol. 2009;21:258-65.
[67] Batista FD, Harwood NE. The who, how and where of antigen presentation to B cells. Nature reviews Immunology. 2009;9:15-27.
[68] Cyster JG. B cell follicles and antigen encounters of the third kind. Nat Immunol. 2010;11:989-96.
[69] Catron DM, Pape KA, Fife BT, van Rooijen N, Jenkins MK. A protease-dependent mechanism for initiating T-dependent B cell responses to large particulate antigens. J Immunol. 2010;184:3609-17.
[70] Kim J, Mooney DJ. In Vivo Modulation of Dendritic Cells by Engineered Materials: Towards New Cancer Vaccines. Nano Today. 2011;6:466-77.

[71] Klippstein R, Pozo D. Nanotechnology-based manipulation of dendritic cells for enhanced immunotherapy strategies. Nanomedicine. 2010;6:523-9.
[72] Misharin AV, Morales-Nebreda L, Mutlu GM, Budinger GR, Perlman H. Flow cytometric analysis of macrophages and dendritic cell subsets in the mouse lung. Am J Respir Cell Mol Biol. 2013;49:503-10.
[73] Mukai Y, Yoshinaga T, Yoshikawa M, Matsuo K, Yoshikawa T, Matsuo K, et al. Induction of endoplasmic reticulum-endosome fusion for antigen cross-presentation induced by poly (gamma-glutamic acid) nanoparticles. J Immunol. 2011;187:6249-55.
[74] Wagner S, Jasinska J, Breiteneder H, Kundi M, Pehamberger H, Scheiner O, et al. Delayed tumor onset and reduced tumor growth progression after immunization with a Her-2/neu multi-peptide vaccine and IL-12 in c-neu transgenic mice. Breast Cancer Res Treat. 2007;106:29-38.
[75] Jasinska J, Wagner S, Radauer C, Sedivy R, Brodowicz T, Wiltschke C, et al. Inhibition of tumor cell growth by antibodies induced after vaccination with peptides derived from the extracellular domain of Her-2/neu. Int J Cancer. 2003;107:976-83.
[76] Dakappagari NK, Pyles J, Parihar R, Carson WE, Young DC, Kaumaya PT. A chimeric multi-human epidermal growth factor receptor-2 B cell epitope peptide vaccine mediates superior antitumor responses. J Immunol. 2003;170:4242-53.
[77] Wu GJ, Bruening G. Two proteins from cowpea mosaic virus. Virology. 1971;46:596-612.
[78] Irvine DJ, Hanson MC, Rakhra K, Tokatlian T. Synthetic Nanoparticles for Vaccines and Immunotherapy. Chem Rev. 2015;115:11109-46.
[79] Noad R, Roy P. Virus-like particles as immunogens. Trends in Microbiology. 2003;11:438-44.
[80] Ruedl C, Schwarz K, Jegerlehner A, Storni T, Manolova V, Bachmann MF. Virus-like particles as carriers for T-cell epitopes: limited inhibition of T-cell priming by carrier-specific antibodies. J Virol. 2005;79:717-24.
[81] Da Silva DM, Pastrana DV, Schiller JT, Kast WM. Effect of preexisting neutralizing antibodies on the anti-tumor immune response induced by chimeric human papillomavirus virus-like particle vaccines. Virology. 2001;290:350-60.
[82] Scheerlinck JP, Greenwood DL. Virus-sized vaccine delivery systems. Drug Discov Today. 2008;13:882-7.
[83] Sakurai H, Kawabata K, Sakurai F, Nakagawa S, Mizuguchi H. Innate immune response induced by gene delivery vectors. Int J Pharm. 2008;354:9-15.
[84] Wang W, Erbe AK, Hank JA, Morris ZS, Sondel PM. NK Cell-Mediated Antibody-Dependent Cellular Cytotoxicity in Cancer Immunotherapy. Front Immunol. 2015;6:368.
[85] Stewart R, Hammond SA, Oberst M, Wilkinson RW. The role of Fc gamma receptors in the activity of immunomodulatory antibodies for cancer. Journal for ImmunoTherapy of Cancer. 2014;2:29.
[86] Nimmerjahn F, Ravetch JV. Fcgamma receptors as regulators of immune responses. Nature reviews Immunology. 2008;8.
[87] Wen AM, Lee KL, Yildiz I, Bruckman MA, Shukla S, Steinmetz NF. Viral nanoparticles for in vivo tumor imaging. Journal of visualized experiments : JoVE. 2012:e4352.